Monthly Notices
of the
ROYAL ASTRONOMICAL SOCIETY

MNRAS **432,** 1319–1329 (2013) doi:10.1093/mnras/stt545
Advance Access publication 2013 April 28

VLBI observations of the shortest orbital period black hole binary, MAXI J1659−152

Z. Paragi,[1]⋆ A. J. van der Horst,[2] T. Belloni,[3] J. C. A. Miller-Jones,[4] J. Linford,[5] G. Taylor,[5] J. Yang,[1] M. A. Garrett,[6,7] J. Granot,[8] C. Kouveliotou,[9] E. Kuulkers[10] and R. A. M. J. Wijers[11]

[1]*Joint Institute for VLBI in Europe, Postbus 2, NL-7990 AA Dwingeloo, the Netherlands*
[2]*Astronomical Institute 'Anton Pannekoek', University of Amsterdam, Postbus 94249, NL-1090 GE Amsterdam, the Netherlands*
[3]*INAF – Osservatorio Astronomico di Brera, Via E. Bianchi 46, I-23807 Merate, Italy*
[4]*International Centre for Radio Astronomy Research – Curtin University, GPO Box U1987, Perth, WA 6845, Australia*
[5]*Department of Physics and Astronomy, University of New Mexico, MSC07 4220, Albuquerque, NM 87131-0001, USA*
[6]*Netherlands Institute for Radio Astronomy (ASTRON), Postbus 2, NL-7990 AA Dwingeloo, the Netherlands*
[7]*Leiden Observatory, University of Leiden, PO Box 9513, NL-2300 RA Leiden, the Netherlands*
[8]*Departement of Natural Sciences, The Open University of Israel, PO Box 808, Ra'anana 43537, Israel*
[9]*Space Science Office, NASA/Marshall Space Flight Center, Huntsville, AL 38512, USA*
[10]*European Space Astronomy Centre (ESA/ESAC), Science Operations Department, E-28691 Villanueva de la Cañada, Madrid, Spain*
[11]*Astronomical Institute, University of Amsterdam, Science Park 904, NL-1098 XH Amsterdam, the Netherlands*

Accepted 2013 March 27. Received 2013 March 27; in original form 2012 September 4

ABSTRACT

The X-ray transient MAXI J1659−152 was discovered by *Swift*/Burst Alert Telescope and it was initially identified as a gamma-ray burst. Soon its Galactic origin and binary nature were established. There exists a wealth of multiwavelength monitoring data for this source, providing a great coverage of the full X-ray transition in this candidate black hole binary system. We obtained two epochs of European very long baseline interferometry (VLBI) Network (EVN) electronic-VLBI and four epochs of Very Long Baseline Array data of MAXI J1659−152 which show evidence for outflow in the early phases. The overall source properties (polarization, milliarcsecond-scale radio structure, flat radio spectrum) are described well with the presence of a compact jet in the system through the transition from the hard–intermediate to the soft X-ray spectral state. The apparent dependence of source size and the radio core position on the observed flux density (luminosity-dependent core shift) supports this interpretation as well. We see no evidence for major discrete ejecta during the outburst. For the source proper motion we derive 2σ upper limits of 115 μas d^{-1} in right ascension, and 37 μas d^{-1} in declination, over a time baseline of 12 d. These correspond to velocities of 1400 and 440 km s^{-1}, respectively, assuming a source distance of ∼7 kpc.

Key words: stars: individual: MAXI J1659−152 – ISM: jets and outflows – X-rays: binaries.

1 INTRODUCTION

Galactic black hole X-ray binaries (BHXRBs) are key to understanding the power sources of accreting compact objects and the physical processes of accretion and jet formation. A great number of these systems have been identified as transient X-ray sources, and sometimes they are referred to as microquasars (Mirabel et al. 1992; Mirabel & Rodríguez 1994), owing to their ability to produce collimated, highly relativistic ejecta analogous to those powered by supermassive black holes in the centres of active galactic nuclei (AGN). There are two types of jets in BHXRBs: compact, synchrotron self-absorbed jets that are typical of the canonical hard spectral state (e.g. Dhawan, Mirabel & Rodríguez 2000; Stirling et al. 2001), and transient ejecta during X-ray state transitions from the hard state to the soft state, crossing a region in the X-ray luminosity versus X-ray hardness space often referred to as the 'jet-line' (Fender, Belloni & Gallo 2004; Fender, Homan & Belloni 2009). Whether there is a universal jet-line region for all BHXRBs, what its boundaries are, and most importantly, what the underlying physics is, remain a matter of debate.[1] Most notably, we point out

⋆E-mail: zparagi@jive.nl

[1] A recent result shows that the location of the jet line may vary from outburst to outburst in a single object (Miller-Jones et al. 2012).

that high angular resolution observations on milliarcsecond (mas) scales have rarely been available in the past, although there has been an increasing number of very long baseline interferometry (VLBI) observations in the past 5 yr, thanks in part to the more flexible, real-time electronic-VLBI (e-VLBI) operations of the European VLBI Network (EVN; see e.g. Tudose et al. 2007). Using the e-VLBI technique with the EVN to observe transients has the advantage of the quick turnaround time, providing more efficient ways to schedule follow-up EVN and/or Very Long Baseline Array (VLBA) observations, as previously demonstrated for various types of transients (Miller-Jones et al. 2010; Paragi et al. 2010a; Moldon, Ribó & Paredes 2011; Yang et al. 2011). The rapid feedback is important for a better understanding of the evolution of the mas-scale source properties early on during the outburst event (especially for transients with no firm identification at their discovery). It also gives the opportunity, as we demonstrate in this paper, to test observing strategies and look for closer VLBI calibrators for targets with less favourable locations, such as low-declination ($<-10^{\circ}$) sources for the EVN. The focus of this paper is a new BHXRB, which benefited from both.

On 2010 September 25 *Swift*/Burst Alert Telescope (BAT) discovered a new transient, which was initially identified as a gamma-ray burst (GRB) and was designated as GRB 100925A (Mangano et al. 2010). The Monitor of All-sky X-ray Image (MAXI)/Gas Slit Camera (GSC) team detected a hard X-ray transient positionally coincident with this GRB candidate, and catalogued it as MAXI J1659−152 (Negoro et al. 2010). Soon it became clear from optical spectroscopy by the European Southern Observatory (ESO)/Very Large Telescope (VLT) X-shooter that the transient showed broad emission and absorption lines at zero redshift, indicating that the source was likely a Galactic X-ray binary (de Ugarte Postigo et al. 2010). The source followed an evolutionary track on the X-ray hardness–intensity diagram (HID) and also had variability/timing properties typical of BHXRBs, in particular type-B and type-C quasi-periodic oscillations (QPO; Kalamkar et al. 2011). The X-ray light curves from *Swift*, *XMM–Newton* and *RXTE* showed irregularly shaped dips that recurred with a period of ∼2.4 h, making the source the shortest orbital period Galactic black hole binary candidate known (Kennea et al. 2011; Kuulkers et al. 2012). The two groups that reported these results also showed that the companion star is most likely an M5 dwarf, and that the system is likely located at a distance of 7 kpc (but see Section 4.1). In addition, using the scaling relation between the spectral index and the QPO frequency, the mass of the black hole is estimated to be 20 ± 3 $M_{\odot}$ (Shaposhnikov et al. 2012). If this estimate is correct, then MAXI J1659−152 would be the most massive stellar black hole known in the Galaxy.

The apparent high distance from the Galactic plane ($z = 2.4 \pm 1.0$ kpc) makes MAXI J1659−152 a good candidate for being a 'runaway microquasar' (Yamaoka et al. 2012; Kuulkers et al. 2013), which received a large kick velocity during the formation of the black hole in the system. With high resolution VLBI observations one could in principle measure the proper motion even during a single outburst, as was demonstrated by Mirabel et al. (2001) in the case of XTE J1118+480. The claimed mass of 20 ± 3 $M_{\odot}$ for MAXI J1659−152 (Shaposhnikov et al. 2012) is incompatible with the runaway microquasar scenario, therefore, constraining the proper motion with VLBI is particularly interesting in this case. However, for rapidly evolving outbursts, the short time-scales can make such a measurement quite challenging.

Just ∼1.5 d after the initial trigger, MAXI J1659−152 was detected at the 5 mJy level at 5 GHz with the Westerbork Synthesis Radio Telescope (WSRT; van der Horst et al. 2010a). This was rapidly followed by a series of EVN e-VLBI (Paragi et al. 2010b) and VLBA target of opportunity observations at 5 GHz. This paper summarizes the results of all the VLBI observations. We describe the initial e-VLBI experiment with the selection of secondary calibrators, and the follow-up EVN and VLBA observations in Section 2. Data reduction and results will be presented in Section 3. The compact jet model, as a framework for the interpretation of the mas-scale structure, is presented in Section 4. In Section 5, we compare the mas-scale properties of MAXI J1659−152 to those of other BHXRBs with similar evolution on an X-ray HID. Conclusions will be drawn in Section 6.

2 OBSERVATIONAL STRATEGY AND SECONDARY CALIBRATOR SELECTION

The first observation of MAXI J1659−152 was carried out on 2010 September 30 with the EVN at 5 GHz in real-time e-VLBI mode with the EVN MkIV Data Processor ('e-EVN'; experiment code RP016A). After the initial clock searching and set-up checking, the project started at 13:00 UT and lasted 5.5 h. The participating telescopes were Effelsberg, Medicina, Onsala, Toruń, the phased array WSRT, Jodrell Bank (MkII), Cambridge and Hartebeesthoek. The data rate per telescope was 1024 Mbps, except for Medicina, Hartebeesthoek (both 896 Mbps) and Cambridge [128 Mbps, limited by the Multi-Element Radio Linked Interferometer Network (MERLIN) microwave link to Jodrell Bank]. We used 2-bit sampling and observed both left and right circular polarizations. The target was phase referenced to the nearby calibrator J1707−1415 ($2\overset{\circ}{.}2$ away), selected from the VLBA Calibrator list.[2] The coordinates used for correlation of the phase reference source were α(J2000) = 17:07:20.390556 ($\pm 0.25/\cos(\delta)$ mas) and δ (J2000) = −14:15:23.12829 (±0.5 mas).

Because of the low declination of the field, the source elevations were low, especially for the EVN: the maximum elevation for most EVN telescopes was around 20°, and it was below 20° at some telescopes for a significant fraction of the observing time. This limits the accuracy of determining the interferometer phase for the target using calibrator measurements. The coherence time is shorter, and systematic errors due to small deviations from the correlator delay model result in errors in the astrometry, as well as decreasing the fidelity of the final image. At the frequency of our observations, tropospheric and ionospheric phase errors have comparable effect on the data, however, at low elevations the tropospheric errors will likely dominate. Both at the EVN and the VLBA correlators the tropospheric delays are determined from a zenith value which is then mapped to lower elevations. A small error in the tropospheric zenith delay, imperfections in the mapping function itself or inhomogeneities in the troposphere will lead to a significant differential phase error between the calibrator and the target close to the horizon. This results in correlation amplitude losses, degraded image fidelity and poor astrometry. The closer the reference source, the smaller the differential phase errors between the reference and the target fields.

Therefore we looked for additional radio sources closer to MAXI J1659−152. Unfortunately, this field is not covered by the Very Large Array (VLA) B-array Faint Images of the Radio Sky at Twenty-cm (FIRST) survey (Becker, White & Helfand 1995), which is an excellent resource to look for potential secondary

[2] http://www.vlba.nrao.edu/astro/calib/index.shtml

calibrators for VLBI observations (Frey et al. 2008). Instead, we selected eight radio sources from the VLA D-array NRAO VLA Sky Survey (NVSS; Condon et al. 1998) that were located within half a degree of the target and had total flux densities exceeding 10 mJy. These were cross-checked against our 5 GHz WSRT data (from ongoing total flux density monitoring). One target, NVSS J170003.28−145622.9 (hereafter J1700−1456) had a nearly flat spectrum. We included this source in the EVN observing schedule to verify its compact structure on mas scales. The phase referencing cycle was 90 s on J1707−1415 and 150 s on MAXI J1659−152. Approximately every 16 min we also observed the secondary calibrator J1700−1456. Additional calibrators OQ 208, J1724−1443, J1751+0939 and J1310+3220 were observed for a short time to check amplitude calibration of the EVN; 3C 286 was included for calibrating the WSRT synthesis array data recorded parallel to the VLBI observations. After the successful detection of both the transient and J1700−1456 (see Section 3.) we carried out further VLBI observations, all at 5 GHz. However, in the case of J1700−1456 we quickly updated the coordinates because they were found to be in error by about 1 arcsec, which is a significant fraction of the WSRT phased-array beam at 5 GHz. The second epoch was observed with the VLBA (BV070A) on October 2. The VLBA data were recorded at the telescopes at a recording rate of 512 Mbps, in dual-polarization mode using 2-bit sampling, and were correlated with DiFX (Deller et al. 2011). The third epoch was observed with the e-EVN on October 4 (RP016B), with a similar set-up to the first experiment but adding the 40-m Yebes telescope to the array. Because MAXI J1659−152 was still detectable with very long baselines (Paragi et al. 2010b), additional VLBA observations were organized (BV070B-D) on 2010 October 6, 14 and 19, until the transient faded below the detection threshold of our WSRT monitoring. The time between observing epochs was set based on the initial e-EVN results and the X-ray spectral and timing properties as observed by *RXTE*.

3 DATA REDUCTION AND RESULTS

The EVN and the VLBA data were reduced according to the standard procedures outlined in the EVN Data Analysis Guide[3] and the AIPS Cookbook,[4] respectively. After the initial amplitude calibration, parallactic angle correction (EVN) and earth orientation parameter correction (VLBA), the data were fringe-fitted in AIPS. At the first three epochs, when MAXI J1659−152 was still brighter than 1 mJy, we also looked for polarized emission in the VLBI data. We performed cross-hand fringe-fitting on a bright calibrator to remove the interchannel R–L delay and phase offsets at the reference antenna. For the EVN data we used OQ 208, whereas for the first epoch VLBA data set we used NRAO 530. We then imaged and self-calibrated OQ 208 in DIFMAP (Shepherd, Pearson & Taylor 1994), and the self-calibrated OQ 208 data were used to determine the antenna polarization leakage terms with LPCAL in AIPS (for both the EVN and VLBA data). The phases of both the science target and the secondary calibrator were phase referenced to J1707−1415. The secondary calibrator, J1700−1456, was imaged and self-calibrated in DIFMAP. This source has resolved structure on a scale of a few mas (see Fig. 1). In the higher resolution VLBA data, the average position of the maximum brightness peak in the brighter, south-western component is α(J2000) = 17:00:03.333340 and δ (J2000) = −14:56:21.97584. The statistical error from the four measurements

[3] http://www.evlbi.org/user_guide/guide/userguide.html
[4] http://www.aips.nrao.edu/CookHTML/CookBook.html

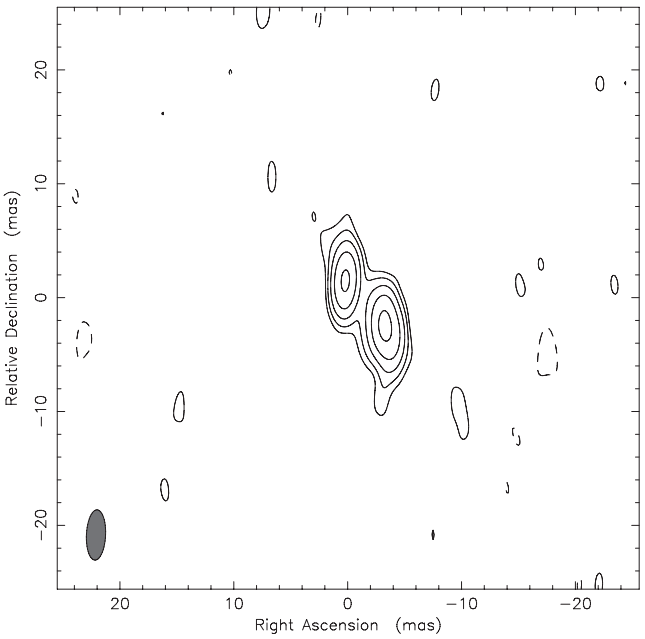

Figure 1. Naturally weighted 5 GHz VLBA map of J1700−1456 on 2010 October 2. This source was found to be compact in the first e-EVN observations and was used as a secondary phase-reference calibrator at the following epochs. The higher resolution VLBA observations show a double structure on mas scales, but the signal-to-noise ratio was still sufficient for additional phase calibration after the residual fringe delay, rate and phase solutions were derived using the primary reference source J1707−1415, which lies further away from the target. The peak brightness is 4.5 mJy beam^{-1}. The contour levels are −1, 1, 2, 4, 8 and 16 times 230 μJy beam^{-1}. The restoring beam is 4.4×1.7 mas, with major axis PA = −2°.6 E of N.

is 170 μas in right ascension and 250 μas in declination. Accounting for the positional error of the primary phase-reference source, this increases to 320 and 560 μas, respectively.

The image was imported back into AIPS where phase solutions were derived with CALIB using a solution interval of 30 min, and applied to the target. This step helped to improve the image fidelity of the target, as well as the astrometric precision of the results. Note that we used the highest quality VLBA map to self-calibrate all epochs, except for the first epoch EVN data because the accurate coordinates of J1700−1456 were not known during the correlation of the first experiment, therefore, exact alignment of the VLBA and the first epoch EVN phase centres is not possible below the ∼mas level. Choosing a 30 min solution interval ensured that we corrected for a smoothly changing residual phase resulting from the imperfect troposphere model, rather than short time-scale phase fluctuations. In the case of the EVN, we did not solve for Cambridge and Hartebeesthoek because they had low signal-to-noise ratios on J1700−1456. In addition, at the first epoch the secondary calibrator phase errors were higher than expected for the WSRT, likely because the a priori position had an error of about an arcsecond, which is a significant fraction of the phased-array WSRT beam. In that case the WSRT phases (only) were self-calibrated on the target, which had a comparable total flux density to the secondary calibrator at the first epoch. This additional phase self-calibration, using a 30 min solution interval, did not significantly affect the final result. The final images of the target were made in DIFMAP, with no further self-calibration at the other epochs.

In the following discussion we utilize the fact that MAXI J1659−152 had a flat spectrum during the first two EVN

epochs. As part of a broad-band monitoring campaign, the source was observed with the Karl G. Jansky VLA at multiple frequencies on 2010 September 29 and October 1. On the former date the flux density was 9.88 ± 0.30 mJy at 4.9 GHz and 10.03 ± 0.31 mJy at 8.5 GHz, while on the latter date those were 10.29 ± 0.32 and 9.74 ± 0.30 mJy, respectively. The resulting spectral indices are 0.03 ± 0.11 and −0.10 ± 0.11, consistent with an index of 0. We note that there are no significant detections of polarization at those epochs, with upper limits of a few per cent on the degree of polarization. Further details on the VLA data analysis can be found in van der Horst et al. (in preparation).

3.1 Results

The resulting VLBI maps are shown in Fig. 2, and the map parameters and model-fit results are listed in Table 1. At the first epoch on 2010 September 30 the source is well resolved, as also clearly evidenced by the decreasing visibility amplitude with increasing baseline length seen in the *uv* data, especially on the most sensitive baselines that include either Effelsberg or Westerbork. Fitting a single elliptical Gaussian model component to the *uv* data gives a total flux density of 8.7 mJy and a characteristic size of 8 mas (well exceeding the uniformly weighted beam size including all baselines), elongated at PA ∼ 132° (measured from north through east). Analysing the Westerbork synthesis array data taken during the VLBI observations, the total flux density of MAXI J1659−152 was 9.8 mJy, i.e. the single component contains most of the flux density from the target. To recover all of the WSRT total flux density, three model components were fitted to the data (see Table 1). Note that the naturally weighted EVN images shown in Fig. 2 do not include the baselines to Hartebeesthoek, for better reconstruction of the extended emission. The uniformly weighted image including Hartebeesthoek data suggests there is extension to the south-east on mas scales, in agreement with the model-fit results. This image contains a total cleaned flux density of 6.3 mJy. The naturally weighted image on the other hand has a total cleaned flux density of 9.6 ± 0.1 mJy, recovering practically all of the integrated flux density. It shows an extension roughly to the east up to 20 mas. It is hard to judge from these data alone whether the apparent extension to the west-north-west is real or not, but this feature agrees in orientation with the major axis PA of the fitted elliptical Gaussian component.

The higher resolution VLBA image on October 2 shows a partially resolved central component containing 6.3 mJy. Fitting a single elliptical Gaussian component resulted in a major axis of PA ∼ 115°, close to the single-component fit EVN value. There is extended emission on both sides of the source roughly in this direction. This extended emission is only detected on the shortest spacings. But since it does not disappear even with further point source model phase self-calibration, and the overall structure is similar to the EVN result, we conclude that the extended emission is likely real. The source was therefore fitted with three circular Gaussian components, with a total flux density of 8.8 mJy. By the second EVN observation, on October 4, the total flux density of MAXI J1659−152 had decreased to 2.95 mJy according to our WSRT measurement. We fitted a circular Gaussian brightness distribution model directly to the *uv* data. The entire integrated flux density was recovered this way in a single component (consistent with the WSRT value within the errors), with a radius of 1.1 mas. MAXI J1659−152 was detected in two more VLBA observations. Although the source looks compact in the images from epochs 3 and 4, the source was still resolved according to our model-fit results (see Table 1). At the fifth epoch the fitted Gaussian component size was smaller than the theoretical resolution limit of our array, therefore, we consider the minimum resolvable angular size as an upper limit (see Lobanov 2005). MAXI J1659−152 faded below the detection level of 300 μJy beam^{-1} (5σ) on 2010 October 19.

No polarized emission was detected at any of these epochs. The first EVN epoch, with the highest peak in total intensity and lowest noise in polarized intensity, provides the strongest constraint. The 150 μJy beam^{-1} upper limit (5σ) in polarized intensity corresponds to a 2.5 per cent upper limit in fractional polarization.

Using the higher resolution VLBA data, the derived average position for MAXI J1659−152 is α (J2000) = 16:59:01.676891 and δ (J2000) = −15:15:28.73237. The error in declination is 220 μas, consistent with the measured errors in the secondary reference source position. In right ascension the error is much larger, 690 μas. The peak in the (lower resolution) first epoch EVN map is about 2 mas east of the average position. This is unusual since due to calibration errors at low elevations, one expects to see larger errors in declination than in right ascension (cf. Yang et al. 2012). Therefore, this is likely the sign of a source structural effect. The October 4 EVN position is within the 2σ error. The total errors in α and δ, including the uncertainty in the primary phase-reference source position, are 740 and 550 μas, respectively.

4 DISCUSSION

4.1 A compact jet in MAXI J1659−152?

The images in Fig. 2 clearly show resolved or partially resolved structures at the first three epochs, indicative of an outflow. The maximum brightness temperatures resulting from fitting circular Gaussian components to the *uv* data at each epoch range from ∼10^7 to 10^8 K (see Table 1). These high brightness temperatures, together with the observed flat radio spectrum (see Section 3), are indicative of optically thick synchrotron radiation, which is also consistent with the observed low fractional polarization (<2.5 per cent). An optically thick synchrotron spectrum may originate in partially self-absorbed compact jets (for details see Appendix). In fact, such partially self-absorbed compact jets have been resolved with VLBI in the BHXRB candidate SS 433 (Paragi et al. 1999), and the confirmed BHXRB systems GRS 1915+105 (Dhawan et al. 2000) and Cyg X-1 (Stirling et al. 2001). Various other observational evidence points to the fact that in general, BHXRBs produce compact jets in the canonical hard X-ray state (Fender et al. 2004, 2009). Our highest resolution data do not show a resolved core–jet structure, but the images from the first two epochs clearly show extensions roughly to the east and to the north-west, that may be related to an outflow. The model-fitting results are also consistent with an elongated structure in a similar direction. One explanation for the overall fuzzy appearance of the 'core' could be angular broadening of the images due to interstellar scattering. Definitive evidence for scatter broadening would be multifrequency measurements that showed a ν^{-2} dependence of the observed source size. However, the nearby secondary calibrator source J1700−1456 showed no evidence for scatter broadening.

We have two other pieces of circumstantial evidence for supporting the self-absorbed jet nature for the bulk of the radio emission. Curiously, MAXI J1659−152 appeared to be the most compact at the last detection on 2010 October 14, when the total flux density was less than 1 mJy. At earlier epochs (and especially with the larger EVN beam) a larger overall source size was measured because of the extended emission (outflow). The radius of maximum brightness temperature, and consequently the measured size of the

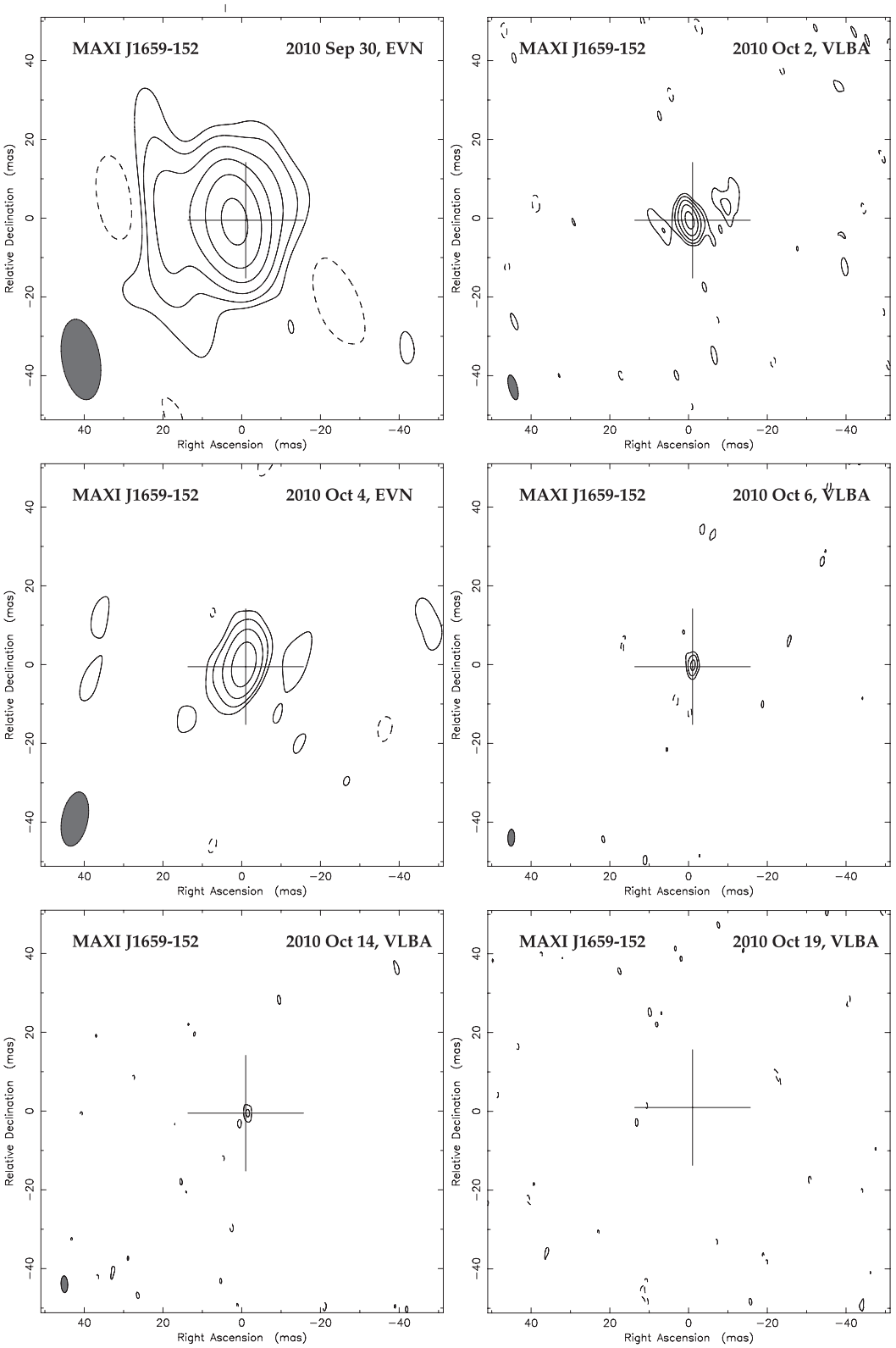

Figure 2. Naturally weighted 5 GHz EVN and VLBA images of MAXI J1659-152. The coordinates of the map centres are α(J2000) = 16:59:01.676959, δ (J2000) = −15:15:28.73200. The peak brightnesses are (in time order) 6.2, 3.9, 2.5, 0.9, 0.4 and 0.2 (non-detection) mJy beam^{-1}. The contour levels are powers of two times the 3σ noise level, typically 170 μJy beam^{-1}. The cross indicates the average VLBA position. Map parameters are listed in Table 1.

Table 1. Map parameters for Fig. 2 as well as model-fit results and brightness temperatures for all observations at 5 GHz. The columns are the following: observing array; observation start date [dd.mm.yyyy]; Modified Julian Date of the midpoint of the observations; peak brightness (mJy beam^{-1}); noise (mJy beam^{-1}); restoring beam major and minor axes (mas), position angle (°; note the last epoch map is a dirty map, therefore, a restoring beam is not given); model-fitted circular Gaussian component flux density (mJy); radius (mas) and the corresponding (lower limit to the) brightness temperature.

Array	Date	MJD	Peak (mJy beam^{-1})	Noise (mJy beam^{-1})	Major (mas)	Minor (mas)	PA (°)	S (mJy)	Radius (mas)	T_b (10^7 K)
EVN	30.09.2010	55469.7	6.24	0.052	20.70	9.67	9.55	7.31	5.3	1.4
								1.88	13.0	0.1
								0.46	2.0	0.6
VLBA	02.10.2010	55472.0	3.92	0.060	6.45	2.15	14.6	6.25	2.4	6.0
								1.58	6.1	0.2
								0.99	4.7	0.2
EVN	04.10.2010	55473.7	2.45	0.062	14.00	6.58	−11.4	2.72	1.1	12.5
VLBA	06.10.2010	55474.0	0.87	0.057	4.28	1.71	−1.9	1.07	1.0	5.9
VLBA	14.10.2010	55484.0	0.40	0.056	4.25	1.70	2.64	0.45	<0.7	>4.7
VLBA	19.10.2010	55489.0	<0.30	0.057	N/A	N/A	N/A	<0.30	N/A	N/A

compact jet region, depends on the radio luminosity (Blandford & Königl 1979). The measured size values from Table 1 are plotted in the left-hand panel of Fig. 5 as a function of flux density. While the scatter is significant, there seems to be a trend of increasing angular size with increasing flux density, as expected for compact jets. The different array configurations of the EVN and VLBA observations probably affect the size measurements, so we cannot compare the size–flux dependence with model predictions. The important point here is that changes in total jet power or bulk Lorentz factor will change the source flux as well as apparent size: initially the source brightens and grows, but as the flare fades it shrinks – this is not expected in cases where the radio emission is related to discrete ejecta or a shell of matter that was ejected from the system.

A strong dependence of size with flux density was previously found in another microquasar, Cyg X-3 (Newell, Garrett & Spencer 1998). In that case the authors claimed to have observed superluminal expansion and contraction on time-scales of hours. Another similarity is that while a collimated radio jet is clearly present during outbursts of Cyg X-3 (e.g. Mioduszewski et al. 2001), the optically thick base morphologically does not resemble a core–jet structure. Instead, it looks like the 'fuzzy' core of MAXI J1659−152. In the case of Cyg X-3, the scatter-broadening effect is well established, with a scattering disc size of ∼18 mas at 5 GHz (Mioduszewski et al. 2001). However, the explanation of scattering is inconsistent with the small size we measured in the last epoch. This same argument (i.e. the measured source size being smaller than the scattering size) could also imply that Newell et al. (1998) may not have measured actual physical sizes, thereby weakening the claim for apparent superluminal expansion in Cyg X-3 (Mioduszewski et al. 2001). In the case of MAXI J1659−152, a scattering screen, if present, must be well localized at the target position because scatter broadening is not observed in the nearby calibrators.

Besides the apparent correlation between the source core flux density and its size, we compare the dependence of the apparent core position with the variable core size, because in compact jets these are intimately related. In Fig. 3 we show the intensity profile for a simple compact jet model (see Appendix). The observed radio core position as well as its apparent size change with observing frequency. This is because at different frequencies the optical depth is different; an effect known as the frequency-dependent core shift in AGN (Lobanov 1998). The true position of the black hole is not easy to determine with high accuracy. Hada et al. (2011) used multifrequency observations to pinpoint the location of the jet base in

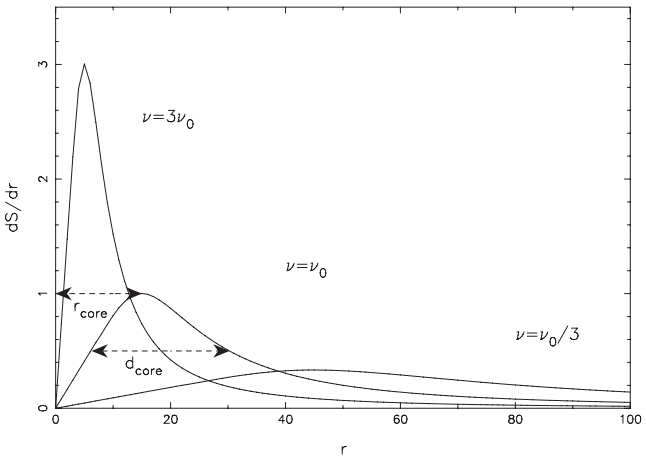

Figure 3. The jet intensity profile with distance from the central engine. Both dS/dr and r are in arbitrary units. r_{core} is the distance between the jet origin (∼the compact object) and the brightest peak of the compact jet. It demonstrates that the observed 'radio cores' of microquasars and AGN do not exactly coincide with the location of the black hole. d_{core} is the FWHM size of the compact jet profile (approximately the size of the source obtained by fitting a Gaussian profile to the uv data). The model is scaled so that the optical depth is unity at distance $r = 20$, at reference frequency ν_0. Jet parameters are $m = 1$, $n = 2$, $s = 2$ ($k_r = 1$, $k_\tau = 3$). For an explanation of the different jet parameters, see Appendix A.

M87, and they concluded that the supermassive black hole is within 14–23 Schwarzschild radii of the 43 GHz radio core (a projected angular separation of 41 μas). The only similar measurement for Galactic microquasars was made in SS 433. Paragi et al. (1999) used the well-established kinematic model of the ballistically moving, optically thin jet components to locate the binary system in between the approaching and receding sides of the optically thick radio core components. The separation between the binary system and the observed radio core position decreased with increasing frequency, i.e. they observed the frequency-dependent core shift in a Galactic microquasar.

Because we observed MAXI J1659−152 at a single frequency, we cannot probe the frequency-dependent core shift. However, any change of optical depth during an outburst (due to e.g. an increase in relativistic particle number density and/or an increase in the magnetic field strength) will result in a similar effect when we compare

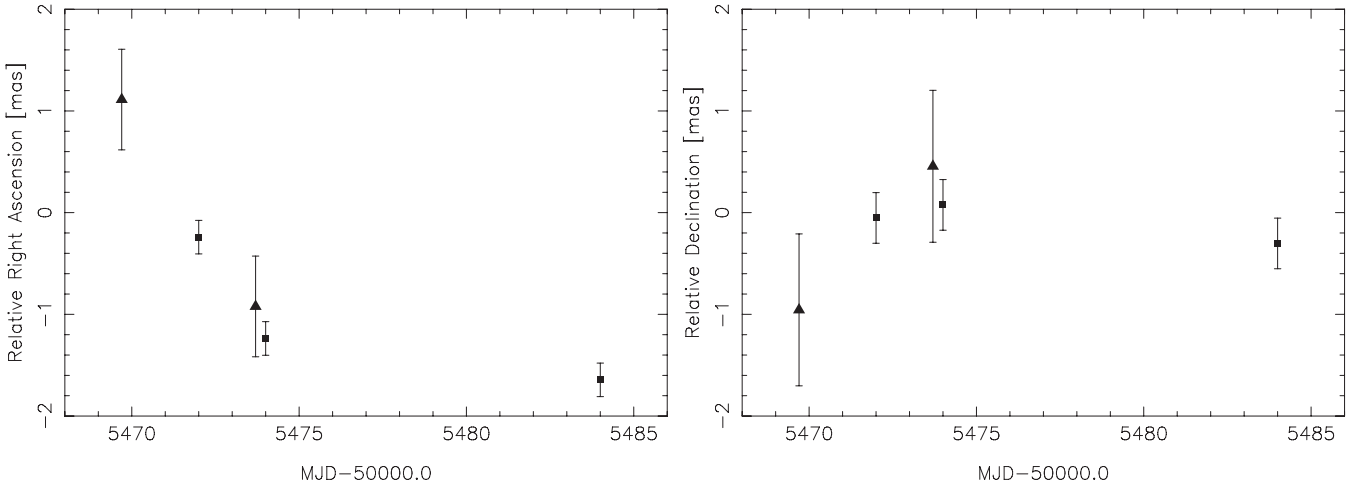

Figure 4. Map peak position relative to the map centre in right ascension ($\alpha\cos\delta$; left-hand panel) and declination (δ; right-hand panel), as measured at 5 GHz at the various epochs. The EVN measurements are indicated by triangles, the VLBA ones with squares. There is a clear, smooth change in right ascension during the VLBI monitoring programme, most likely related to structural changes in the emission. The increasing negative offset in right ascension shows a gradual shift of the source peak emission to the west. There is no clear variation in declination, and the measurements agree within the errors.

core positions and sizes at various epochs at a single frequency. This will result in a larger separation of the observed peak radio emission and the compact object, and at the same time a larger observed size for the compact jet. This effect can be probed with VLBI at a single frequency, even if, as mentioned above, the core shift, $r_{\rm core}$, cannot be measured in most cases. By simply scaling our model with the initial optical depth, we find that $r_{\rm core}$ is roughly proportional to the full width at half-maximum (FWHM) of the jet profile, $d_{\rm core}$, in which case the difference of peak positions Δr will be proportional to the difference of the measured core sizes Δd between the various epochs. In Fig. 4 we plot the relative peak positions of MAXI J1659−152. Note the apparent positions in right ascension continuously drift from roughly east towards the west at the various epochs, indicating either proper motion or varying source structure. Because the first epoch map clearly shows an extension to the east, it is plausible that we see a shrinking compact jet as the source flux density decreases. In the right-hand panel of Fig. 5 we plot the difference in core position versus difference in core size, with respect to the first epoch. The data show a smooth change in source size along with a smooth change in core (more precisely, compact jet peak) position in a way that is compatible with the expected relation between $r_{\rm core}$ and $d_{\rm core}$ for compact jets. Monitoring VLBI observations of similar transients at multiple frequencies can potentially confirm these effects: the core size and position change with luminosity(luminosity-dependent core shift), as well as with observing frequency (frequency-dependent core shift, shown in Fig. 3).

On the other hand, one may interpret the positional change as source proper motion. Here we take a conservative approach. Because the first epoch was clearly affected by source structure and

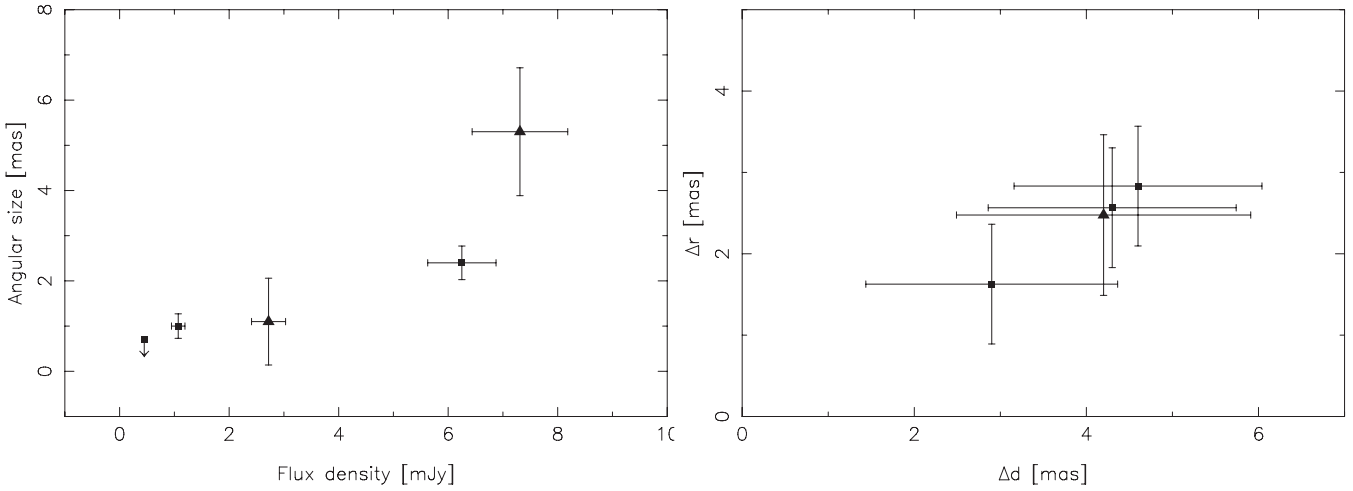

Figure 5. The left-hand panel shows the source size of MAXI J1659−152 (circular Gaussian component fit; we used the dominant core components at the first two epochs) as a function of its flux density at 5 GHz (triangles: EVN; squares: VLBA). In the right-hand panel we show the observed 'core' position change (Δr) versus the measured source size change (Δd) relative to the first epoch. From a simple scaling of the opacity in our compact jet model, it is expected that the position of the peak emission and the FWHM width of the compact jet scale linearly with one another. Therefore, by analogy with the frequency-dependent core shift (see Fig. 3), one may measure a time-dependent core shift at a fixed frequency during an outburst, and compare it to the observed change in core size. The data seem to show the expected trend. Admittedly, the number of measurements is small, and the errors are large (triangle: EVN; squares: VLBA).

the time baseline is very short, we give a 2σ upper limit of 1380 μas in right ascension and 440 μas in declination; in 12 d (epochs 2–5), these correspond to proper motion upper limits of $\mu_\alpha < 115$ μas d^{-1} and $\mu_\delta < 37$ μas d^{-1}.[5] To convert these to velocities, we have to know the source distance, which is not strongly constrained, as is typically the case for X-ray transients. Based on the relation between optical outburst amplitude and the orbital period in similar systems (Shahbaz & Kuulkers 1998), Kuulkers et al. (2012) estimated a distance of 7 ± 3 kpc for MAXI J1659-152. As pointed out by Miller-Jones et al. (2011), this does not take into account the effect of orbital inclination to the line of sight; at high inclinations the observed brightness of the disc would be underestimated, and consequently, the derived distance would be an overestimate. In a subsequent paper, Kuulkers et al. (2013) derived an updated distance of 8.6 ± 3.7 kpc, using the original amplitude–period relation. Correcting for the inclination angle of the orbit, the distance would be lowered to 7.1 ± 3.0 kpc at $i = 65^\circ$, and 4.0 ± 1.7 kpc at $i = 80^\circ$. The corresponding heights above the Galactic plane are $z = 2.4 \pm 1.1$, 2.0 ± 0.9 and 1.1 ± 0.5 kpc, respectively (Kuulkers et al. 2013). Our VLBI images do not show a highly beamed source structure, with a very compact core and one-sided ejection, and they do not show symmetric double-sided ejecta in the plane of the sky either. Assuming that the jets are perpendicular to the accretion disc, this would mean that the orbit of the binary is likely moderately inclined to the line of sight, preferring the ∼7 kpc value. Finally, by carefully taking into account various arguments, Jonker et al. (2012) estimated a source distance of 6 ± 2 kpc, although this error bar may be underestimated given the number of assumptions involved.

Assuming a distance of 7 kpc, our proper motion constraints correspond to upper limits on the space velocity of $\lesssim$1400 km s^{-1} in right ascension and $\lesssim$440 km s^{-1} in declination. In the high-inclination angle case (corresponding to a distance of 4 kpc), these numbers would change to ∼800 and ∼250 km s^{-1}, respectively. These values are not particularly constraining, since there are no measured black hole kicks as large as 1400 km s^{-1}. Yamaoka et al. (2012) argued that MAXI J1659−152 is a runaway microquasar, just like XTE J1118+480, which has a velocity of 145 km s^{-1} with respect to the local standard of rest (Mirabel et al. 2001). Kuulkers et al. (2013) concluded that this was a likely scenario for MAXI J1659−152 because shorter period (less massive) systems should have the highest runaway velocities; this scenario would also explain the large distance from the Galactic plane. Our 12 d time baseline was too short to significantly constrain the velocity. With the accurate coordinates measured during this outburst, future VLBI observations in the next activity cycle will give an accurate space velocity measurement for MAXI J1659−152. For future X-ray transients with a more prolonged flaring activity, it will be possible to use this method to probe the runaway microquasar scenario if the transient is within a few kpc. Further improvement on the positional accuracy can be obtained if one can find a secondary calibrator closer to the target, especially one within the primary beam of the telescopes. But as we have seen in here, varying source structure will likely be a limiting factor in most cases.

[5] We note that in order to minimize the structural effects in right ascension, one could use the last two VLBA detections to constrain the proper motion in right ascension, when the source was most compact. Although the time baseline is somewhat shorter (9 d), the measured statistical errors in right ascension for the secondary calibrator are also smaller. Using these we would arrive at a very similar proper motion constraint in right ascension as in declination.

4.2 X-ray properties and radio structure

The observed radio structure of MAXI J1659−152 is consistent with a compact jet, which is typical for the canonical hard state of BHXRBs. We will now consider the X-ray properties of the transient. The *RXTE* light curve and HID (6–15 keV/2–6 keV) are shown in Fig. 6; black points show measurements closest to the VLBI epochs. The source already left the canonical hard state and was in the hard intermediate state (HIMS) by the time of the first EVN epoch. The presence of a compact jet in the HIMS state is not unprecedented; Cyg X-1 is known to show a compact jet in this state. During the evolution to the soft intermediate state (SIMS), radio quenching was reported from MAXI J1659−152 on October 8 (van der Horst et al. 2010b) and type-B QPOs appeared on October 12 (Muñoz-Darias et al. 2011), which are usually followed by relativistic jet ejections. Note that radio quenching and subsequent bright, discrete ejecta are typical of BHXRBs during their transition to the soft state. However, while our measurements confirm the radio quenching, we do not see discrete ejecta in MAXI J1659−152. Instead, the source simply faded below our detection limit. Because of the relatively rapid cadence (∼2 d) of our observations during the radio bright state of the source, and because no other flaring events were reported from total flux density monitoring campaigns, it is quite unlikely that we missed an ejection event. We note also that our final VLBA observation was taken when the source was in its softest X-ray state (see Fig. 6), and by that time the *RXTE* count rate was well into its decay phase, therefore, we do not expect significant radio flaring after this time. The lack of ejecta may indicate that MAXI J1659−152 underwent a failed transition. However, as was shown by Muñoz-Darias et al. (2011), the X-ray state transition was fully completed, according to the well-established criteria: the total rms variability went down to almost 1 per cent, unlike H1743−322. It is true however that the soft state in MAXI J1659−152 was very short lived and appeared significantly harder than that in most BHXRBs. Muñoz-Darias et al. (2011) proposed that this may be due to the high inclination of the system, in which case we see less of the soft disc emission while the emission from the spherical, non-thermal corona should be largely inclination independent. A similar lack of bright, transient ejecta was reported for the transition of Cyg X-1 to the soft state in 2010 June (Rushton et al. 2012). However, Cyg X-1 is also peculiar in that it has a non-canonical soft state (significantly higher fractional rms variability than typical transient BHXRB outbursts). VLBI observations of many more transient events are necessary to draw general conclusions about the formation of transient ejecta, whether they appear in all soft-state transitions, and where exactly the 'jet-line' is located in the HID (which may vary from system to system, and even within a given system; Miller-Jones et al. 2012).

Jonker et al. (2012) discuss the well-known radio–X-ray correlation in BHXRBs (e.g. Corbel et al. 2003; Gallo, Fender & Pooley 2003; Jonker et al. 2004). During the canonical hard state, the observed correlation is $L_\mathrm{R} \propto L_\mathrm{X}^{0.6}$; more recently it has been shown that a number of systems follow a much steeper correlation with $L_\mathrm{R} \propto L_\mathrm{X}^{1.4}$ (Coriat et al. 2011; Gallo, Miller & Fender 2012). At the beginning of its outburst, while the luminosity was in excess of 10^{36} erg s^{-1}, Jonker et al. (2012) found MAXI J1659-152 to follow the steeper correlation, but to be significantly more radio luminous at a given X-ray luminosity than the rest of the sources on the steeper correlation track. To explain this discrepancy, they proposed that the source either falls on the outlier branch, but with suppressed X-ray luminosity owing to the high inclination, or that the radio emission was possibly dominated by optically thin ejecta

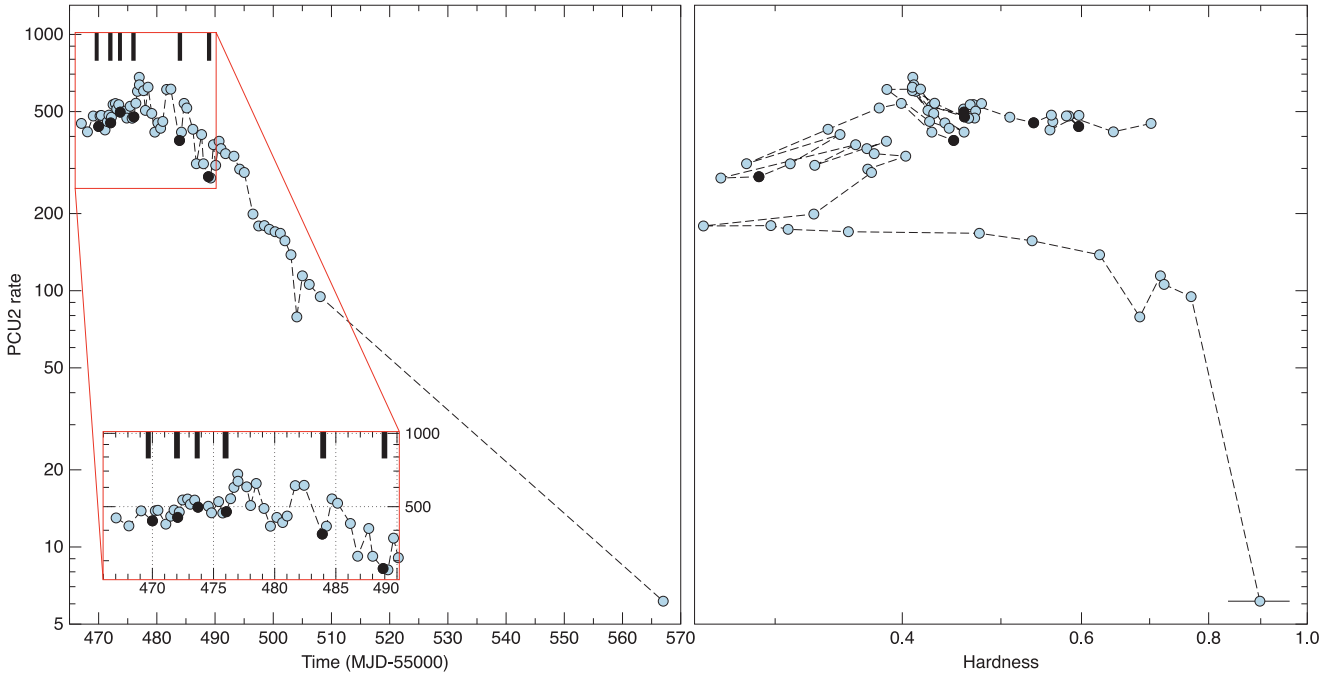

Figure 6. *RXTE* PCU2 count rate (2–20 keV, left) and HID of MAXI J1659−152 during its outburst in 2010. The hardness is defined as the ratio of count rates measured in the 6–15 and the 2–6 keV energy ranges. The black bars indicate the times of the VLBI observations while the black circles show the *RXTE* measurements closest in time to the VLBI observations.

at early times, increasing the average radio luminosity. In contrast, in fig. 9 of Corbel et al. (2013), MAXI J1659-152 does not appear to be significantly radio overluminous for the steeper correlation track. A re-examination of the original data of Jonker et al. (2012) revealed a discrepancy in the assumed distance of H1743−322, the single source that best defines the steeper correlation track (Coriat et al. 2011). Assuming instead the accepted distance of 8 kpc for H1743−322, MAXI J1659−152 would no longer appear significantly radio overluminous (Jonker, private communication). However, this does not address an additional motivation for the possibility of optically thin radio flares namely the reported detection of a high level of linear polarization from a preliminary analysis of WSRT data (van der Horst et al. 2010a). Reanalysis of these WSRT data however showed no significant linear polarization (see Section 3), in agreement with our VLBI results, which show no evidence for optically thin ejecta. The small observed physical size, the flat spectrum, the lack of significant proper motion and the low linear polarization suggest that the radio emission was dominated by a compact jet.

5 CONCLUSIONS

We presented a series of VLBI (real-time e-VLBI at the EVN plus VLBA) monitoring results for the BHXRB candidate MAXI J1659−152. The VLBI maps show evidence for an outflow on a scale of 10 mas. The compact jet scenario fits the data well: the low polarization, flat spectrum as well as the observed source size and luminosity-dependent core shift all support this interpretation. During the full phase transition from the HIMS through the SIMS to the soft state, we do not see evidence for the luminous, discrete ejecta that are typical for BHXRBs in this state, possibly indicating that the outflow rate was not sufficient to form powerful shocks, as seen in the case of Cyg X-1. As Yamaoka et al. (2012) and Kuulkers et al. (2013) pointed out, MAXI J1659−152 could potentially be a runaway microquasar. Further VLBI observations during another outburst will be necessary to measure the proper motion of the system with high accuracy. With the method presented here, it should be possible to provide useful constraints on black hole transient proper motions even during a single outburst if the outburst lasts long enough. The runaway microquasar hypothesis could then be tested.

ACKNOWLEDGEMENTS

We thank the anonymous referee for the constructive comments, which helped to improve our paper significantly. ZP thanks to Andrei Lobanov for discussions about the compact jet model. e-VLBI research infrastructure in Europe is supported by the European Union's Seventh Framework Programme (FP7/2007-2013) under grant agreement RI-261525 NEXPReS. JCAMJ acknowledges support from an Australian Research Council Discovery Grant (DP120102393). The EVN is a joint facility of European, Chinese, South African and other radio astronomy institutes funded by their national research councils. The WSRT is operated by Netherlands Institute for Radio Astronomy (ASTRON) with support from the Netherlands Foundation for Scientific Research. The National Radio Astronomy Observatory is a facility of the National Science Foundation operated under cooperative agreement by Associated Universities, Inc. This work made use of the Swinburne University of Technology software correlator, developed as part of the Australian Major National Research Facilities Programme and operated under license. The research leading to these results has received funding from the European Community's Seventh Framework Programme (FP7/2007-2013) under grant agreement ITN 215212.

REFERENCES

Becker R. H., White R. L., Helfand D. J., 1995, ApJ, 450, 559
Blandford R. D., Königl A., 1979, ApJ, 232, 34

Blandford R. D., Rees M. J., 1974, MNRAS, 169, 395
Condon J. J., Cotton W. D., Greisen E. W., Yin Q. F., Perley R. A., Taylor G. B., Broderick J. J., 1998, AJ, 115, 1693
Corbel S., Nowak M. A., Fender R. P., Tzioumis A. K., Markoff S., 2003, A&A, 400, 1007
Corbel S., Coriat M., Brocksopp C., Tzioumis A. K., Fender R. P., Tomsick J. A., Buxton M. M., Bailyn C. D., 2013, MNRAS, 428, 2500
Coriat M. et al., 2011, in Romero G. E., Sunyaev R. A., Belloni T., eds, Proc. IAU Symp. 275, Jets at all Scales. Cambridge Univ. Press, Cambridge, p. 255
Deller A. T. et al., 2011, PASP, 123, 275
de Ugarte Postigo A., Flores H., Wiersema K., Thoene C. C., Fynbo J. P. U., Goldoni P., 2010, GRB Coordinates Network, Circular Service, 11307
Dhawan V., Mirabel I. F., Rodríguez L. F., 2000, ApJ, 543, 373
Fender R. P., Belloni T. M., Gallo E., 2004, MNRAS, 355, 1105
Fender R. P., Homan J., Belloni T. M., 2009, MNRAS, 396, 1370
Frey S., Gurvits L. I., Paragi Z., Mosoni L., Garrett M. A., Garrington S. T., 2008, A&A, 477, 781
Gallo E., Fender R. P., Pooley G. G., 2003, MNRAS, 344, 60
Gallo E., Miller B., Fender R. P., 2012, MNRAS, 423, 590
Georganopoulos M., Marscher A. P., 1996, in Hardee P. E., Bridle A. H., Zensus J. A., eds, ASP Conf. Ser. Vol. 100, Energy Transport in Radio Galaxies and Quasars. Astron. Soc. Pac., San Francisco, p. 67
Hada K., Doi A., Kino M., Nagai H., Hagiwara Y., Kawaguchi N., 2011, Nat, 477, 185
Hjellming R. M., Han X., 1995, in Lewin W. H. G., van Paradijs J., van den Heuvel E. P. J., eds, Cambridge Astrophys. Ser. Vol. 26, X-ray Binaries. Cambridge Univ. Press, Cambridge, p. 326
Hjellming R. M., Johnston K. J., 1988, ApJ, 328, 600 (HJ88)
Jonker P. G., Gallo E., Dhawan V., Rupen M., Fender R. P., Dubus G., 2004, MNRAS, 351, 1359
Jonker P. G., Miller-Jones J. C. A., Homan J., Tomsick J., Fender R. P., Kaaret P., Markoff S., Gallo E., 2012, MNRAS, 423, 3308
Kalamkar M., Homan J., Altamirano D., van der Klis M., Casella P., Linares M., 2011, ApJ, 731, L2
Kennea J. A. et al., 2011, ApJ, 736, 22
Königl A., 1981, ApJ, 243, 700
Kuulkers E. et al., 2012, in Mihara T., Serino M., eds, 4th International MAXI Workshop, IPCR CR-127, The First Year of MAXI: Monitoring Variable X-ray Sources. Aoyama Gakuin University, Tokyo, p. 81
Kuulkers E. et al., 2013, A&A, 552, A32
Lobanov A. P., 1998, A&A, 330, 79
Lobanov A. P., 2005, preprint (astro-ph/0503225)
Mangano V., Hoversten E. A., Markwardt C. B., Sbarufatti B., Starling R. L. C., Ukwatta T. N., 2010, GRB Coordinates Network, Circular Service, 11296
Miller-Jones J. C. A. et al., 2010, ApJ, 716, L109
Miller-Jones J. C. A., Madej O. K., Jonker P. G., Homan J., Ratti E. M., Torres M. A. P., 2011, Astron. Telegram, 3358
Miller-Jones J. C. A. et al., 2012, MNRAS, 421, 468
Miodusze wski A. J., Rupen M. P., Hjellming R. M., Pooley G. G., Waltman E. B., 2001, ApJ, 553, 766
Mirabel I. F., Rodríguez L. F., 1994, Nat, 371, 46
Mirabel I. F., Rodríguez L. F., Cordier B., Paul J., Lebrun F., 1992, Nat, 358, 215
Mirabel I. F., Dhawan V., Mignani R. P., Rodrigues I., Guglielmetti F., 2001, Nat, 413, 139
Moldon J., Ribó M., Paredes J. M., 2011, A&A, 533, L7
Muñoz-Darias T., Motta S., Stiele H., Belloni T. M., 2011, MNRAS, 415, 292
Negoro H. et al., 2010, Astron. Telegram, 2873
Newell S. J., Garrett M. A., Spencer R. E., 1998, MNRAS, 293, L17
Paragi Z., Vermeulen R. C., Fejes I., Schilizzi R. T., Spencer R. E., Stirling A. M., 1999, A&A, 348, 910
Paragi Z. et al., 2010a, Nat, 463, 516
Paragi Z. et al., 2010b, Astron. Telegram, 2906
Rushton A. et al., 2012, MNRAS, 419, 3194
Rybicki G. B., Lightman A. P., 1979, Radiative Processes in Astrophysics. Wiley-Interscience, New York
Shahbaz T., Kuulkers E., 1998, MNRAS, 295, L1
Shaposhnikov N., Swank J. H., Markwardt C., Krimm H., 2012, in Mihara T., Serino M., eds, 4th International MAXI Workshop, IPCR CR-127, The First Year of MAXI: Monitoring Variable X-ray Sources. Aoyama Gakuin University, Tokyo, p. 51
Shepherd M. C., Pearson T. J., Taylor G. B., 1994, BAAS, 26, 987
Stirling A. M., Spencer R. E., de la Force C. J., Garrett M. A., Fender R. P., Ogley R. N., 2001, MNRAS, 327, 1273
Tudose V. et al., 2007, MNRAS, 375, L11
van der Horst A. J., Granot J., Paragi Z., Kouveliotou C., Wijers R. A. M., Ramirez-Ruiz E., 2010a, Astron. Telegram, 2874
van der Horst A. J. et al., 2010b, Astron. Telegram, 2918
Yamaoka K. et al., 2011, PASJ, 64, 32
Yang J., Paragi Z., Corbel S., Gurvits L. I., Campbell R. M., Brocksopp C., 2011, MNRAS, 418, L25
Yang J. et al., 2012, MNRAS, 426, L66

APPENDIX A: COMPACT JET MODEL

A conical jet model to describe the intensity profile of the radio jets in the galactic XRB SS433 was developed by Hjellming & Johnston (1988, hereafter HJ88). Here we follow HJ88, but instead of the large-scale jet we will concentrate on the properties of the optically thick inner core, also taking into account more general considerations for the variation of magnetic field with distance, as done for case of AGN jet models (see below). Let us assume a conical and freely expanding jet with radius proportional to the distance r to the central engine. Synchrotron radiation is emitted by electrons moving in a tangled magnetic field with average strength B. We assume that the energy spectrum of the radiating electrons – filling the entire volume of the jet – has a power law form, $N(\gamma_e) \sim \gamma_e^{-s}$, where s is the energy spectral index, which is generally thought to be $\sim$2 ($1.0 \lesssim s \lesssim 3.0$ will be considered in the present paper). The optically thin spectrum of the source will have a spectral index $\alpha = (1 - s)/2$ ($S \propto \nu^{\alpha}$; e.g. Rybicki & Lightman 1979). The magnetic field and the particle density are assumed to depend on r as $B \propto r^{-m}$ and $N \propto r^{-n}$; for a conical geometry, m can vary between 1 and 2 (Blandford & Rees 1974). If $m = 1$ and $n = 2$, the energy density of the magnetic field and the kinetic energy density of the electrons are in equipartition at any r along the flow (Blandford & Königl 1979). All quantities determined below are expressed in the emitting frame of the fluid.

The optical depth to synchrotron radiation through the jet axis can be written as (cf. Lobanov 1998)

$$\tau(r) = \tau_0 (r/r_0)^{-k_r(\epsilon+1)} (\nu/\nu_0)^{-(\epsilon+1)}, \tag{A1}$$

where $\epsilon = (s + 2)/2$ and $k_r = (\epsilon m + n - 1)/(\epsilon + 1)$. For the equipartition values of $m = 1$ and $n = 2$, $k_r = 1$ independent of the energy spectral index. In this case the optical depth scales as $r^{-(\epsilon+1)}$ and the location of the radio core is inversely proportional to the observing frequency (Blandford & Königl 1979). The actual value of the constant τ_0 depends on the selection of r_0 and θ, the jet inclination to the line of sight (assumed to be constant).

Following HJ88, the contribution to the flux density of a portion of the jet of length dr can be written as

$$\frac{\mathrm{d}S}{\mathrm{d}r} = C \sin\theta \, (\nu/\nu_0)^{5/2} \, (r/r_0)^{(m+2)/2} \, (1 - \mathrm{e}^{-\tau}) \, \xi_{\mathrm{con}}(\tau), \tag{A2}$$

where $\xi_{\mathrm{con}} = a + b\tau - c\tau^2 \ldots$ is the geometrical correction function for conical jets and $a, b, c, \ldots$ constants are given by Hjellming & Han (1995). The actual value of the constant C is determined by

the opening angle of the flow, the magnetic field strength and number density of electrons etc., at a reference distance r_0. Note that equations (A2) and (A1) are more general than that given originally by HJ88, since m and n are not fixed. These values, together with the energy spectral index s – through k_r – determine the shape of the jet intensity profile (see Fig. 3).

The jet intensity first rises sharply with r and reaches its maximum at $r = r_{\rm core}$ (at a given frequency). Within a few $r_{\rm core}$ its flux density will decrease significantly. One can also determine the brightness variation in the core with frequency. The optically thick limit of the integrated flux density from equation (A2) gives (Königl 1981)

$$\alpha_{\rm core} = 5/2 - (m + 4)/(2k_r). \quad \text{(A3)}$$

While the peak of the jet intensity profile is roughly proportional to the frequency, the integrated spectrum of the core remains flat or slightly inverted, as typically observed in radio-loud AGN. The spectral index can vary in the range $-0.5 \lesssim \alpha \lesssim 1.5$, with the equipartition value of $\alpha = 0.0$.

In our model k_r is assumed to be constant throughout the region of interest (in the core at a given frequency). If k_r changes smoothly with decreasing r (consequently, at increasing ν), then equation (A2) is approximately valid only in a frequency range $\Delta\nu = \nu_2 - \nu_1$, for which k_r is determined. In the inner jets (at $\nu \gg 1$ GHz), however, the geometry of the flow may be different from conical due to external pressure gradients (e.g. Georganopoulos & Marscher 1996) and k_r may change very fast. Clearly, our simple model does not describe this scenario well. External pressure gradients may be caused for example by a dense, optically thick stellar wind. As most of the jet environment is expected to be ionized, this results in additional free–free absorption, and the jet intensity profile will depend also on the distribution of the absorbing medium.

This paper has been typeset from a TEX/LATEX file prepared by the author.